Nanosecond Pulses in a THz Gyrotron Oscillator Operating in a Mode-Locked Self-Consistent Q-Switch Regime

S. Alberti,[1,*] F. Braunmueller,[1] T. M. Tran,[1] J. Genoud,[1] J-Ph. Hogge,[1] M. Q. Tran,[1] and J-Ph. Ansermet[2]

[1]*Centre de Recherches en Physique des Plasmas, Station 13, Ecole Polytechnique Fédérale de Lausanne (EPFL), CH-1015 Lausanne, Switzerland*

[2]*Institute of Condensed Matter Physics, Station 3, EPFL, 1015 Lausanne, Switzerland*

(Received 29 August 2013; published 12 November 2013)

An experimental study of a nanosecond pulsed regime in a THz gyrotron oscillator operating in a self-consistent Q-switch regime has been carried out. The gyrotron is operated in the $TE_{7,2}$ transverse mode radiating at a frequency of 260.5 GHz. The 5 W nanosecond pulses are obtained in a self-consistent Q-switch regime in which the cavity diffraction quality factor dynamically varies by nearly 2 orders of magnitude on a subnanosecond time scale via the nonlinear interaction of different mode-locked frequency-equidistant sidebands. The experimental results are in good agreement with numerical simulations performed with the TWANG code based on a slow time scale formulation of the self-consistent time-dependent nonlinear wave particle interaction equations.

DOI: 10.1103/PhysRevLett.111.205101 PACS numbers: 84.40.Ik, 05.45.−a, 41.60.−m, 52.59.−f

In optical lasers a very well known technique for generating high-power short pulses is based on an externally controlled fast modulation of the cavity quality factor [1]. This technique is called Q switching and relies on the phase locking of many longitudinal frequency-equidistant modes supported by the laser cavity. The most common Q-switch methods employed in optical lasers are based on the transmissivity external control of one of the two mirrors forming the laser cavity and include techniques such as rotating mirror, electro-optic, acousto-optic [1].

In this Letter we report on the first experimental observation of a nanosecond pulsed regime in a 260 GHz gyrotron oscillator, interpreted as the consequence of a self-consistent Q-switch effect in which the diffraction quality factor is dynamically modulated by driving the gyrotron in a strongly nonlinear regime where phase-locked sidebands are excited. In this condition, the Q-switch regime is therefore only a self-consistent result of the nonlinear dynamics and does not require any external control of the system parameters. In the domain of coherent radiation sources based on the interaction of an electron beam and a fast wave, such as it occurs in gyrotrons, nonstationary regimes characterized by the excitation of sidebands have been studied in [2–4]. The mode-locking mechanism has been theoretically and experimentally analyzed in [5,6]. The phase locking of an electron rf oscillator has been proposed in a theoretical paper by Kuzikov and Savilov [7]. For the case of slow-wave electron devices, the theoretical work by Levush *et al.* [8] reports on mode-locking effects. The Q-switch regime has been theoretically studied by Denisov *et al.* [9] for a slow-wave electron backward-wave oscillator and has been experimentally observed in free-electron lasers by Hosaka *et al.* [10].

The detailed description of the experimental setup on which these results are based is presented in [2]. Based on the uncoupled dispersion relation in the $\omega - k_{\|}$ diagram, the operating point where the self-consistent Q-switch (SQS) regime has been observed is shown in Fig. 1. The main system parameters are summarized in the figure caption. Compared to the results given in [2], a further analysis of the electron beam properties with an electron optics code and also a deeper analysis of the nonstationary regimes [11] has confirmed that the pitch angle α is in excess of 1.7–1.9, which is significantly higher than the value given in [2]. We remind the reader that with the triode magnetron injection gun configuration, an independent control of the beam energy and the pitch angle is possible. The studied operating point is indicated with the large red dot in Fig. 1 and is characterized by a zero group velocity corresponding to a zero normalized detuning [2]. Operating points with $k_{\|} < 0$ are in the gyro—backward-wave-oscillator regime (gyro-BWO), characterized by a negative group velocity, whereas points with $k_{\|} > 0$ are in the gyro—traveling-wave-tube regime (gyro-TWT) with a positive group velocity. The beam current is above the threshold for the onset of nonstationary regimes characterized by the appearance of sidebands (automodulation) [2,12]. A detailed characterization of the wide variety of nonstationary regimes has been carried out and is presented in [2,13]. As mentioned above, in this Letter we focus on a specific operating point (see caption of Fig. 1) for which the nanosecond pulsed regime has been observed in its most evident manifestation. There are other neighboring operating points in magnetic field for which the same dynamics has been observed [11].

The key elements for the characterization of the observed fast dynamics is the experimental setup shown in Fig. 2. The fast Schottky diode has been specifically developed by Virginia Diodes Inc. and has a bandwidth from dc to 20 GHz. The intermediate frequency (IF) of the

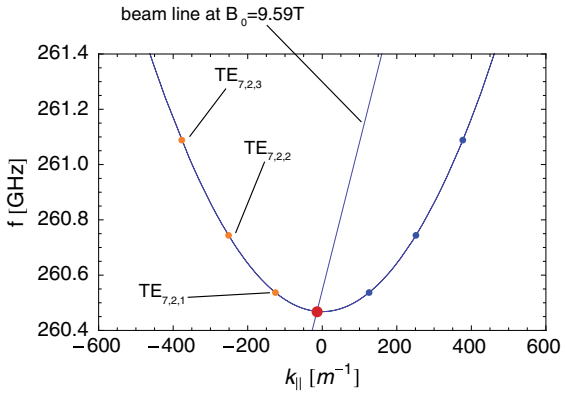

FIG. 1 (color online). Uncoupled dispersion relation in the $\omega - k_\parallel$ space for the operating point exhibiting the self-consistent Q-switch regime. The beam line represents the Doppler shifted electron beam dispersion relation $\omega = \Omega_c + k_\parallel v_\parallel$, with Ω_c, $k_\parallel$, $v_\parallel$ being the relativistic cyclotron angular frequency, the parallel wave vector, and parallel velocity, respectively. The beam energy and pitch angle are 15.5 keV and 1.9, respectively. The cavity magnetic field is $B_0 = 9.59$ T and the beam current is $I_b = 75$ mA. The filled dots on the rf-wave dispersion relation ($TE_{7,2}$ transverse mode) represent the discrete frequencies of longitudinal modes considering a finite length cavity, $L = 25$ mm, with a parallel wave number $k_\parallel = q\pi/L$, with q being the longitudinal index. The large red dot is the SQS operating point.

heterodyne receiver has the same bandwidth as the Schottky diode. The Schottky diode and the IF of the heterodyne receiver time traces are acquired with a fast oscilloscope (Tektronix, model TDS7404). The raw time traces as well as the associated post-treated data for the SQS regime are shown in Fig. 3. As shown in Fig. 3(a), the FWHM of a single rf pulse measured with the Schottky diode is 1.2 ns with a 4.2 ns repetition rate. The time average rf power of $\langle P_{\rm rf}\rangle = 1.2$ W is measured with the calorimeter. Considering the duty cycle and the modulation

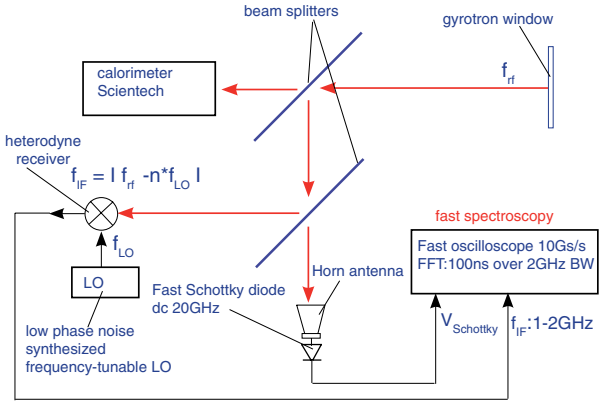

FIG. 2 (color online). Schematic diagram of the experimental setup used for analyzing the THz radiation spectrum. The fast Schottky diode signal is acquired with a fast oscilloscope (10 Gs/s, 8 bit A/D converter) ensuring a time resolution of 100 ps. A low phase noise synthesized local oscillator (LO) drives the harmonic mixer ($n = 24$, $f_{\rm LO} = 10.8$ GHz) of the heterodyne receiver. The IF signal of the heterodyne receiver is acquired at the same acquisition rate. This allows us to perform fast spectroscopy (FFT) with a time resolution of typically 100 ns. Using the beam splitter setup, an absolute measurement of the average gyrotron rf power is made with a Scientech calorimeter (model 360 401).

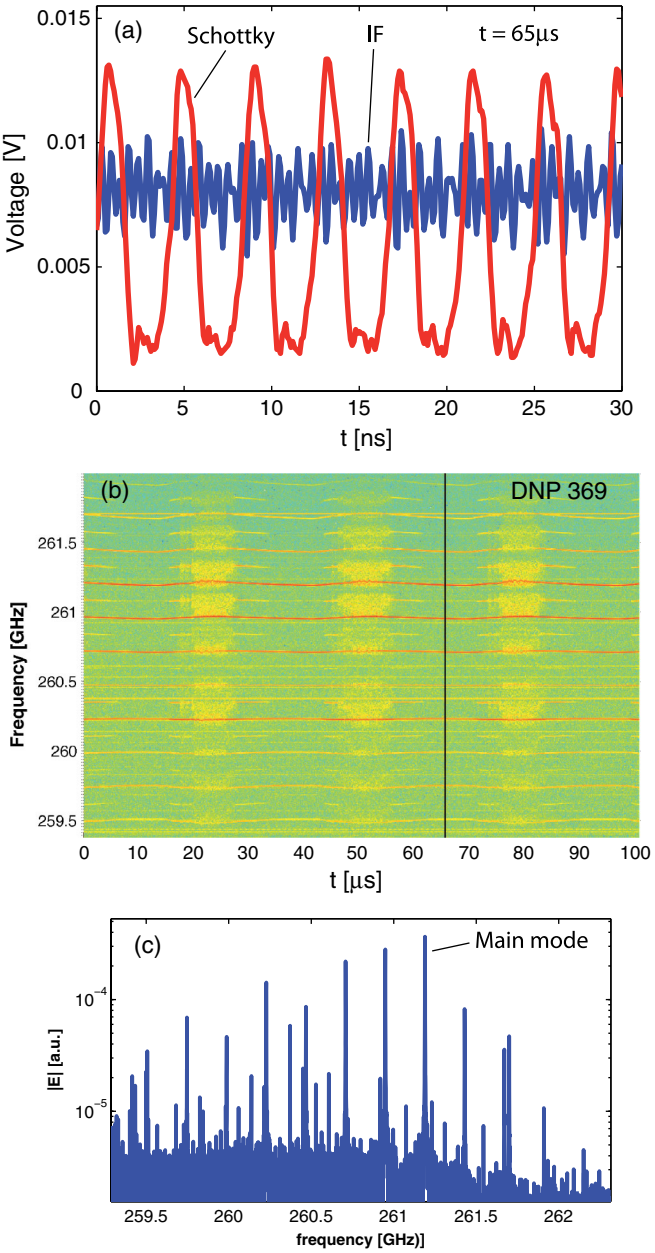

FIG. 3 (color online). Experimental time traces of the SQS regime. (a) In red, fast Schottky diode (dc 20 GHz bandwidth) and, in blue, the IF of the heterodyne receiver. (b) Spectrogram with a time resolution of 100 ns calculated from the IF signal shown in (a). The vertical line indicates the time, $t = 65$ μs, at which the 30 ns time window shown in (a) has been taken. (c) Frequency spectrum (FFT on a 100 ns time window) of the IF signal at $t = 65$ μs. DNP 369 identifies the shot number in the acquisition data base.

depth of 90%, the rf peak power is as high as 5 W. The spectrogram with a 100 ns resolution is shown in Fig. 3(b). It is important to notice that the sidebands are exactly equidistant in frequency with a separation of $\Delta f_{SB} = 240$ MHz [see Fig. 3(b)]. A slight variation of the sideband frequency separation occurs on a slow time scale ($\tau_{anode} \simeq 30\ \mu$s) associated with the anode-voltage fluctuation δV_a. With a relative fluctuation of the anode voltage of $\delta V_a/V_a = 0.3\%$, the corresponding relative fluctuation of the pitch angle is $\delta\alpha/\alpha \simeq 3\%$. The frequency spectrum shown in Fig. 3(c) is calculated using fast Fourier transform (FFT) on a 100 ns time window located at the time shown on the spectrogram and highlights the fact that the sidebands are exactly evenly separated. Using a numerical homodyne detector on an experimentally acquired IF signal, we have determined that the relative phase between the sidebands varies typically by less than 20° over a 5 μs time scale; therefore, the sidebands are mutually phase locked. The pulsed regime shown on the 30 ns time window of Fig. 3(a) is, within some small fluctuations, the same over the full acquisition time window of 100 μs.

For the experimental operating point discussed above, the numerical simulations using the time-dependent self-consistent monomode code TWANG [14] are shown in Fig. 4. In Figs. 4(a)–4(d) the following time traces are represented: the cavity stored energy W, the electronic efficiency η_{el}, the radiation power P_{diff}, and the loaded diffraction quality factor (not taking into account the Ohmic Q) Q_{diff}. The time-dependent loaded diffraction quality factor is calculated as $Q_{diff}(t) = \omega_0 W(t)/P_{diff}(t)$ with the time dependence of $W(t)$ and $P_{diff}(t)$ derived from the time evolution of the rf-field envelope oscillating at the reference frequency ω_0 corresponding to the eigenfrequency of the cold-cavity eigenmode $TE_{7,2,1}$. One clearly observes a deep dynamic modulation of the integral quantities such as W and η_{el} over time scales of the order of the inverse of the sideband frequency separation, $\tau_{mod} = 1/\Delta f_{SB} \simeq 4$ ns. For the two local quantities, P_{diff} and Q_{diff}, an even faster time scale variation is observed. In particular, one notices that in the time window spanning from t_0 to t_2, Q_{diff} varies by nearly 2 orders of magnitude on a subnanosecond time scale. As a reference, the unloaded (cold-cavity) diffractive quality factor for the $TE_{7,2,1}$ mode is $Q_{diff\text{-}cold} = 11800$, and the corresponding total cold-cavity quality factor including diffractive and Ohmic losses is $Q_{tot} = 5100$. Based on these quantities, the cavity filling time is $\tau_{fil} = 2Q_{tot}/\omega = 6.3$ ns. On a time scale much faster than τ_{fil} one notices that in the SQS regime the self-consistent quality factor Q_{diff} dynamically varies between a maximum an order of magnitude higher and a minimum also one order of magnitude lower than the cold-cavity quality factor. Associated with this fast modulation of Q_{diff}, one observes a fast modulation of the radiated power P_{diff} with the maxima and minima indicated by the times t_1 and t_2 shown in Figs. 4(a)–4(d). These

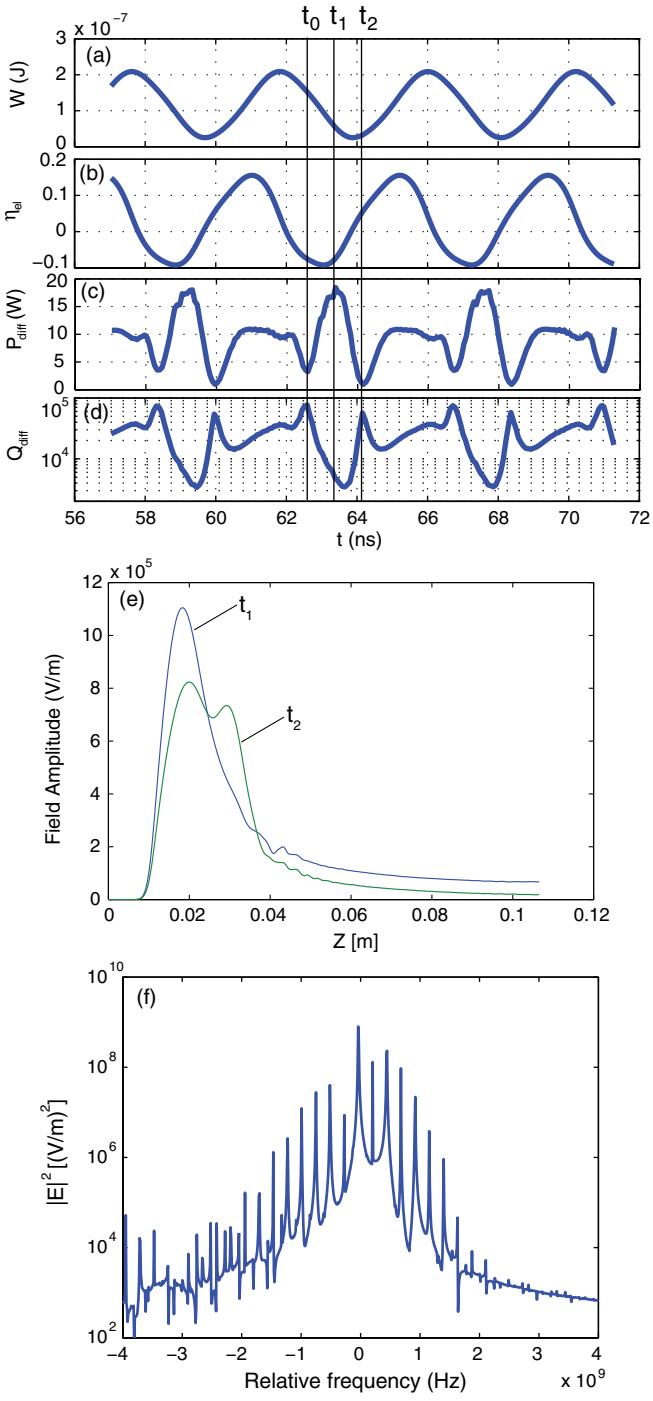

FIG. 4 (color online). Simulation results of the SQS regime calculated with TWANG. The system parameters are the same as for the experiment, and a cavity wall conductivity of $\sigma_{dc} = 2.9 \times 10^7$ [S/m] has been considered. From top to bottom are the time traces of (a) cavity stored rf energy, (b) electronic efficiency, (c) radiated rf power measured at the cavity exit, (d) self-consistent diffraction quality factor. (e) rf-field profile at the times t_1 and t_2 for which the maximum and minimum radiated rf power is predicted. (f) Radiation frequency power spectrum relative to a reference frequency of 260.53 GHz. This spectrum is computed at the exit of the interaction space.

two effects suggest that the observed dynamics is to be associated with a SQS mechanism. The corresponding rf-field profiles calculated at t_1 and t_2 are shown in Fig. 4(e).

Moreover, it has to be noted that the electronic efficiency is strongly modulated during nearly half of the period with a positive efficiency and the second half exhibiting a negative efficiency and, therefore, associated with a situation in which the particles absorb energy from the wave. For the case shown in Fig. 4, it is interesting to note that the strong SQS dynamics occurs during the negative efficiency half-period. The low-order transverse mode $TE_{7,2}$ together with the high rf radiation frequency makes that the Ohmically dissipated power ($\sigma_{dc} = 2.9 \times 10^7$ [S/m]) is also dynamically varying with the same time dependence as the cavity stored energy. The peak Ohmic power, corresponding to the peak cavity stored energy, is as high as 38 W.

Figure 4(f) shows the frequency spectrum calculated at the exit of the interaction space. The frequency axis is referenced to a reference frequency of 260.53 GHz, corresponding to the resonant frequency of the first longitudinal mode, $q = 1$, of the empty cavity. As shown in [2], the reflection coefficient computed at the radiation boundary remains well below 1% over the entire instability bandwidth. One clearly observes that the sidebands are equidistant in frequency and, for the specific operating point, the simulated sideband separation is in excellent agreement with the measured one. It is important to remember that the cold-cavity longitudinal modes are not equidistant since they obey the following equation: $f_q = 1/2\pi\sqrt{\omega_{cut}^2 + (ck_\parallel)^2}$, where ω_{cut} is the cutoff angular frequency for the $TE_{7,2}$ mode and c is the speed of light. Therefore, the different experimentally observed and simulated spectral lines cannot be associated with the excitation of different cold-cavity longitudinal modes.

The sideband frequency separation is estimated in [4] by $\Delta f_{SB\text{-}BWO} \approx 1/(\tau_w + \tau_b)$ for the gyro-BWO case ($k_\parallel < 0$) and by $\Delta f_{SB\text{-}TWT} \approx 1/(2\tau_w)$ for the gyro-TWT case ($k_\parallel > 0$), where τ_w is the wave transit time at the group velocity and τ_b is the electron transit time. These estimations are not derived from first-principles arguments and their applicability strongly depends on the evaluation of the wave group velocity as well as the interaction length L. When applied to our experimental conditions ($\tau_w \simeq$ 0.8–1.2 ns, $\tau_b \simeq 0.7$ ns) the abovementioned estimations give a Δf_{SB} three times larger than the measured value. In Fig. 5 the measured Δf_{SB} versus B_0 is compared to the value predicted by TWANG. One observes that there is a good quantitative agreement between the experiment for a magnetic field region around the operating point of 9.59 T. The points calculated with TWANG below a magnetic field of 9.57 T are not shown since no sidebands are predicted by the code. A significant difference between the simulated and measured Δf_{SB} is observed at higher magnetic field values corresponding to the operation in the gyro-BWO regime. It is to be mentioned that, for the gyro-BWO

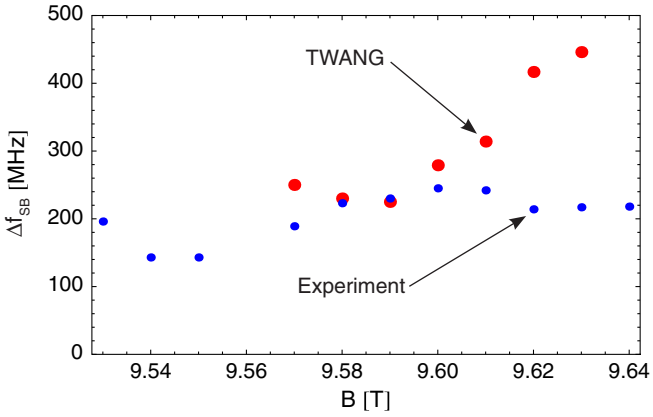

FIG. 5 (color online). For the same electron beam parameters as considered before, but only varying the cavity magnetic field the experiment-theory comparison of the sideband frequency separation is shown. The experimental points are indicated in blue. The theoretical points have been calculated using the TWANG code.

regimes, in which self-consistent effects are dominant, the modeling is often quantitatively less accurate than for the case of the gyrotron oscillators operated in the gyro-TWT regime. Despite the excellent qualitative and often also quantitative agreement between experiment and simulations, it has to be stressed that the underlying model used in the TWANG code is based on the commonly adopted assumption that the electron time of flight in the interaction region τ_b is significantly shorter than the time scale of the electromagnetic field amplitude variation. Under this assumption, the time scale separation allows us to consider that the rf electric field is constant during the electron transit time [15]. From the numerical point of view this allows us to solve independently the electrons' equations of motion and the wave equation at each time step of the time evolution. For a stationary single-frequency operation of the gyrotron, the abovementioned time scale separation can always be satisfied by properly selecting the arbitrary chosen reference frequency as close as possible to the self-consistent frequency. If the spectrum exhibits sidebands (automodulation), this assumption is often violated as is the case for this experiment. With the considered experimental beam parameters, the electron time of flight is $\tau_b \simeq 0.7$ ns, which is comparable to the time scale of the cavity rf-field variation [see Figs. 3(a) and 4(a)–4(d)]. With a particle-in-cell numerical approach, the self-consistent wave particle system of equations would be solved simultaneously at each time step of the evolution and would allow us to properly handle all the relevant time scales.

In summary, we have presented the first experimental demonstration of high-power nanosecond pulses (5 W) in a THz gyrotron oscillator. Based on a theoretical interpretation this pulsed regime is interpreted as a self-consistent Q switch in the presence of mode-locked

sidebands. This novel regime may open up new applications for gyrotrons.

Work supported by Requip (No. 206021-121303/1), Sinergia grants (No. CRSI20-122708/1 and No. 200020-120503/1) of the Swiss National Science Foundation, the Ecole Polytechnique Fédérale de Lausanne (EPFL), and the Faculty of Basic Sciences of EPFL.

*stefano.alberti@epfl.ch

[1] A. E. Siegman, *Lasers* (University Science Books, Sausalito, 1986).
[2] S. Alberti, J.-P. Ansermet, K. A. Avramides, F. Braunmueller, P. Cuanillon, J. Dubray, D. Fasel, J.-P. Hogge, A. Macor, E. de Rijk, M. da Silva, M. Q. Tran, T. M. Tran, and Q. Vuillemin, Phys. Plasmas **19**, 123102 (2012).
[3] T. H. Chang, S. H. Chen, L. R. Barnett, and K. R. Chu, Phys. Rev. Lett. **87**, 064802 (2001).
[4] K. R. Chu, Rev. Mod. Phys. **76**, 489 (2004).
[5] A. H. McCurdy, Appl. Phys. Lett. **66**, 1845 (1995).
[6] J. Zhao, G. Nusinovich, H. Guo, J. Rodgers, and V. Granatstein, IEEE Trans. Plasma Sci. **28**, 597 (2000).
[7] S. V. Kuzikov and A. V. Savilov, Phys. Rev. Lett. **110**, 174801 (2013).
[8] B. Levush, T. M. Antonsen, A. Bromborsky, W. R. Lou, and Y. Carmel, IEEE Trans. Plasma Sci. **20**, 263 (1992).
[9] G. G. Denisov, S. V. Kuzikov, and A. V. Savilov, Phys. Plasmas **18**, 103102 (2011).
[10] M. Hosaka, M. Katoh, A. Mochihashi, J. Yamazaki, K. Hayashi, Y. Takashima, and H. Hama, Nucl. Instrum. Methods Phys. Res., Sect. A **507**, 289 (2003).
[11] F. Braunmueller, J. Genoud, S. Alberti, T. Tran, J.-P. Hogge, Q. Vuillemin, and M. Tran, in Proceedings of the 38th International Conference on Infrared, Millimiter and Terahertz Waves, Mainz, Germany, 2013, paper Mo1-5 (to be published).
[12] N. S. Ginzburg, G. S. Nusinovich, and N. A. Zavolsky, Int. J. Electron. **61**, 881 (1986).
[13] S. Alberti, F. Braunmueller, T. M. Tran, J. Genoud, Q. Vuillemin, J.-P. Hogge, M. Q. Tran, J.-P. Ansermet, A. Macor, and E. de Rijk, in Proceedings of the 38th International Conference on Infrared, Millimiter and Terahertz Waves, Mainz, Germany, 2013, paper Tu1-1 (Ref. [11]).
[14] S. Alberti, T. M. Tran, K. Avramidis, F. Li, and J.-P. Hogge, in *Proceedings of the 36th International Conference on Infrared, Millimiter and Terahertz Waves, Houston, TX, 2011* (IEEE, New York, 2011).
[15] G. S Nusinovich, IEEE Trans. Plasma Sci. **27**, 313 (1999).